Anisotropic magnetoresistance of individual CoFeB and Ni nanotubes with values of up to 1.4% at room temperature

Daniel Rüffer, Marlou Slot, Rupert Huber, Thomas Schwarze, Florian Heimbach, Gözde Tütüncüoglu, Federico Matteini, Eleonora Russo-Averchi, András Kovács, Rafal Dunin-Borkowski, Reza R. Zamani, Joan R. Morante, Jordi Arbiol, Anna Fontcuberta i Morral, and Dirk Grundler

Citation: APL Materials **2**, 076112 (2014); doi: 10.1063/1.4891276

View online: http://dx.doi.org/10.1063/1.4891276

View Table of Contents: http://scitation.aip.org/content/aip/journal/aplmater/2/7?ver=pdfcov

Published by the AIP Publishing

APL MATERIALS **2**, 076112 (2014)

Anisotropic magnetoresistance of individual CoFeB and Ni nanotubes with values of up to 1.4% at room temperature

Daniel Rüffer,[1] Marlou Slot,[1] Rupert Huber,[2] Thomas Schwarze,[2] Florian Heimbach,[2] Gözde Tütüncüoglu,[1] Federico Matteini,[1] Eleonora Russo-Averchi,[1] András Kovács,[3] Rafal Dunin-Borkowski,[3] Reza R. Zamani,[4,5] Joan R. Morante,[5] Jordi Arbiol,[4,6] Anna Fontcuberta i Morral,[1] and Dirk Grundler[2,7,a]

[1]*Laboratoire des Matériaux Semiconducteurs, Institut des Matériaux, Ecole Polytechnique Fédérale de Lausanne, 1015 Lausanne, Switzerland*
[2]*Lehrstuhl für Physik funktionaler Schichtsysteme, Physik-Department, Technische Universität München, D-85747 Garching bei München, Germany*
[3]*Ernst Ruska-Centre for Microscopy and Spectroscopy with Electrons and Peter Grünberg Institute, Forschungszentrum Jülich, D-52425 Jülich, Germany*
[4]*Institut de Ciència de Materials de Barcelona (ICMAB-CSIC), Campus de la UAB, 08193 Bellaterra, CAT, Spain*
[5]*Catalonia Institute for Energy Research (IREC), Barcelona 08930, Spain*
[6]*Institució Catalana de Recerca i Estudis Avançats (ICREA), 08019 Barcelona, CAT, Spain*
[7]*Institut des Matériaux, École Polytechnique Fédérale de Lausanne, 1015 Lausanne, Switzerland*

(Received 25 March 2014; accepted 15 July 2014; published online 30 July 2014)

Magnetic nanotubes (NTs) are interesting for magnetic memory and magnonic applications. We report magnetotransport experiments on individual 10 to 20 μm long Ni and CoFeB NTs with outer diameters ranging from 160 to 390 nm and film thicknesses of 20 to 40 nm. The anisotropic magnetoresistance (AMR) effect studied from 2 K to room temperature (RT) amounted to 1.4% and 0.1% for Ni and CoFeB NTs, respectively, at RT. We evaluated magnetometric demagnetization factors of about 0.7 for Ni and CoFeB NTs having considerably different saturation magnetization. The relatively large AMR value of the Ni nanotubes is promising for RT spintronic applications. The large saturation magnetization of CoFeB is useful in different fields such as magnonics and scanning probe microscopy using nanotubes as magnetic tips. [http://dx.doi.org/10.1063/1.4891276]

Ferromagnetic nanostructures with tubular shape are fascinating objects for fundamental research as well as for applications. Due to their hollow structure, theory predicts the existence of Bloch-point free vortex states and domain walls.[1–3] The motion of vortex domain walls in nanotubes is expected to occur at very high velocities,[4,5] possibly fast enough to generate a Cherenkov-type spin wave excitation.[6] Such magnetic properties and high velocities could be beneficial in future low-power and high-speed memory applications.[7] For this, polycrystalline or even better amorphous materials, being soft-magnetic and magnetically isotropic, represent a very promising basis. While soft-magnetic behavior allows for mobile domain-walls, isotropic magnetic properties are key for the formation of the characteristic magnetic states predicted for tubes. Molecular beam epitaxy and epitaxial growth as reported for GaMnAs, MnAs, and Fe_3Si nanotubes recently[10–12] introduce however magnetocrystalline anisotropy. Magnetron sputtering as a technologically relevant deposition technique has not been reported for the fabrication of magnetic nanotubes yet. Instead

[a]Electronic mail: dirk.grundler@ph.tum.de

ferromagnetic nanotubes were first fabricated by electrodeposition into nanoporous membranes.[13,14] Various other methods were developed such as hydrogen reduction of porous alumina templates preloaded with metallic salts[15] or decomposition of polymers containing a metallo-organic precursor wetting such templates.[16] Different deposition techniques including atomic layer deposition (ALD) were employed to fabricate tubes in nanopores[17,18] or as shells onto semiconductor nanowires.[8,10,17,19] Early magnetic characterization was restricted to large ensembles of nanotubes. In the last years, the investigation of individual nanotubes became technologically feasible.[9,20–24] The role of both magnetocrystalline[9,24] and shape anisotropy[19] has been discussed but the relevant magnetometric demagnetization factor for individual nanotubes has not yet been addressed. For Ni nanotubes anisotropic magnetoresistance (AMR) data presented recently revealed a technologically unfavourable relative AMR effect of only 0.3% at 4 K.[21] Here we report on the structural characterization of polycrystalline Ni and amorphous CoFeB nanotubes. Studying their AMR over a broad temperature range we obtain a large relative effect of up to 1.4% for the Ni nanotubes at room temperature. For both types of nanotubes, we evaluate a consistent magnetometric demagnetization factor $N_{\perp}$ of about 0.7. Thereby we account for the different fields H_{d} needed to saturate the Ni and CoFeB nanotubes in transverse ($\perp$) direction. Correspondingly, the magnetic anisotropy is argued to be dominated by the shape. Large room-temperature AMR values are interesting if one thinks about, e.g., sensor applications or transport studies on magnetic configurations predicted for nanotubes.[1–3] The nanotubes from CoFeB are expected to advance both nanomagnonics and magnetic sensing. Their large saturation magnetization favors fast spin dynamics[25] and provides one with large stray fields from nanoscopic tips, respectively, helping to improve magnetic microscopy.[26]

Magnetic nanotubes were fabricated from either Ni or CoFeB by depositing the ferromagnetic shells around bottom-up grown GaAs nanowires.[27,28] The nanowires, which were grown using Ga droplets as catalysts, had lengths between about 10 and 20 μm. Their diameters ranged from 100 to 150 nm.[27,28] A list of relevant geometrical parameters is given in the table in the supplementary material.[29] The Ni was deposited by ALD,[21,23] while the CoFeB was obtained by magnetron sputtering using Xenon gas at room temperature.[25] In the ALD process, we intentionally produced an intermediate Al_2O_3 layer in order to vary the inner diameter of the supporting core before depositing the ferromagnetic shell. For magnetron sputtering of CoFeB, we mounted the Si (111) substrate containing the GaAs nanowires on a rotatable sample holder facing a $Co_{20}Fe_{60}B_{20}$ (CoFeB) target that was positioned under an angle of 35 ° with respect to the substrate normal. Intentionally choosing ensembles of nanowires with rather large nanowire-to-nanowire separation, the substrate rotation allowed us to obtain nanotubes showing homogeneously thick CoFeB shells.

Annular Dark Field (ADF) Scanning Transmission Electron Microscopy (STEM) images were obtained in order to determine the morphology and thicknesses of the Ni [Fig. 1(a)] and CoFeB shells [Figs. 1(b) and 1(c)]. The Ni shells were found to exhibit a surface roughness with peak-to-peak values of about 10 nm.[21,23] The magnetron-sputtered CoFeB shells were much smoother. Atomic-resolution ADF STEM analyses as those presented in Fig. 1(d) evidenced a zinc-blende structure of the GaAs core that grew along one of the [111]B directions as demonstrated recently.[27,30] Cross sections of the core/shell systems were prepared by means of Focused Ion Beam showing that the hexagonal cross-section of the core was transferred to the CoFeB shell [Fig. 1(c)]. This was not observed for the Ni shells due to the larger surface roughness[21,23] [Fig. 1(a)]. The Ni consisted of grains being ellipsoids with a long (short) axis of roughly 30 nm (10 nm). The conformal CoFeB shell appeared instead amorphous. The amorphous structure is provoked by adding B to the CoFe alloy.[31] The columnar structure seen in Fig. 1(d) is attributed to local variations in the density of the material. These might be caused by directional deposition on the rotating nanowires. This peculiar feature is under further investigation. Electron Energy Loss Spectroscopy (EELS) spectrum images were obtained in STEM mode in order to study the composition. The nanowire cores are composed of GaAs. Shells are shown to be Ni rich in the inset of Fig. 1(a) and Fe and Co rich in Figs. 1(g) and 1(h), respectively. EELS analyses performed on the CoFeB shell provided a relative composition of Fe 77% (at. %), Co 20%, and Xe 3%. Note that the content of B could not be obtained as the energy range of the B in the EELS spectra falls far from the Fe and Co signal. The upper bound for the oxygen content in the shell is determined to be 2%. The values are consistent with energy dispersive x-ray analysis performed on planar films.[25] Remarkably, the catalyst seed for nanowire growth is

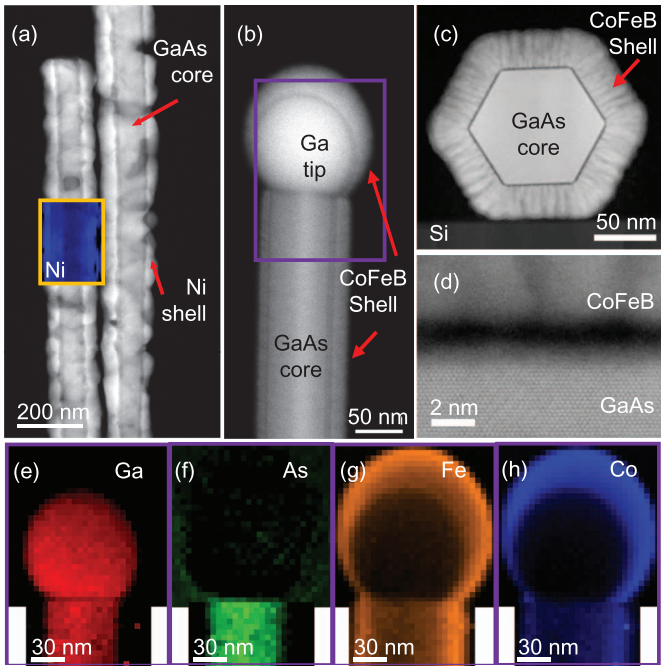

FIG. 1. (a) Low-magnification ADF STEM image of Ni nanotubes; the inset shows an EELS Ni map obtained on the same region of the tube. (b) ADF STEM image of a CoFeB nanotube shell covering the GaAs nanowire template as well as the Ga tip used for bottom-up growth. (c) Cross-section ADF STEM view showing the hexagonal prismatic morphology of the GaAs core template and the CoFeB nanotube shell. (d) Atomic resolution ADF STEM image showing the crystallinity of the GaAs and the amorphous CoFeB shell. The CoFeB exhibits a columnar morphology. The inner ADF detector semi-angle used was 78 mrad. (e)-(h) EELS chemical maps corresponding to Ga, As, Fe, and Co, respectively, obtained on the squared region in (b).

composed of pure Ga covered with a slight thin shell containing As. The CoFeB layer coats the seed as well. In contrast to Refs. 8, 9, and 19, we do not find an epitaxial relationship between the magnetic shells and the semiconductor cores. For polycrystalline Ni and amorphous CoFeB[25,32] prepared on planar substrates a magnetocrystalline anisotropy was not observed.

The core/shell systems were released in isopropanol using sonication and transferred to Si wafers covered with 200 nm thick silicon oxide. The absolute position of nanotubes was determined using prepatterned gold alignment markers, optical microscopy, and an in-house developed software for image recognition.[33] *In situ* plasma etching was performed before sputtering electrical contacts from 5 nm thick titanium and 150 nm thick gold [Fig. 2(b)]. The separation between voltage probes L_{contact} [Fig. 2(c)] was varied between 6.5 and 13.2 μm depending on the investigated nanotube. The Ni nanotubes have a thickness of 40 nm (NiL1, NiL2) and 20 nm (NiM). By inserting an Al_2O_3 layer between the ferromagnetic shell and the GaAs core, we achieved different outer diameters of about 350 nm (large, "L") and 220 nm (middle, "M"). The CoFeB nanotubes considered here have thicknesses of 30 nm (CFBM1, CFBM2) and 20 nm (CFBS1, CFBS2) where "S" (small) indicates an outer diameter of about 180 nm. The CoFeB nanotubes stick to the substrate with one of their side facets.

Magnetotransport experiments were performed on wire-bonded samples mounted on a rotatable stage in a bath cryostat with a superconducting magnet providing a magnetic field $\mu_0 H$ of up to 9 T. The resistance $R(H, \theta)$ as a function of the magnetic field and the rotation angle θ was measured in a four-point-probe configuration [Fig. 2(d)] using a nanovoltmeter in combination with a programmable current source and a three-step current operated at 25 Hz to compensate for thermovoltages. The data from the bath cryostat were corrected for thermal drifts and the field dependent characteristics of the temperature sensor. To compare different nanotubes when rotating a fixed field H, we consider the relative resistance change $\Delta R(\theta) = (R(\theta) - \min(R))/\min(R)$ where

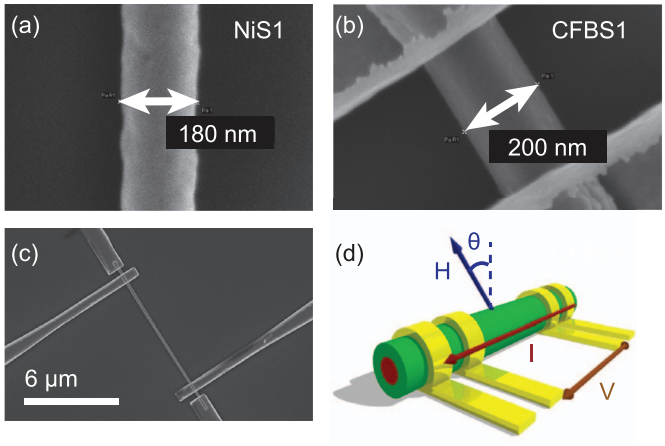

FIG. 2. Scanning electron microscopy images of a small segment of sample (a) NiS1 and (b) CFBS1. (c) Overview of sample CFBS1 with electrical contacts. (d) Measurement configuration.

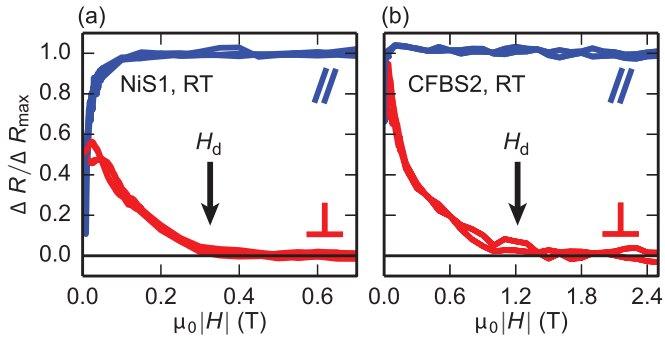

FIG. 3. Normalized resistance change $\Delta R(H)/\Delta R_{max}$ as a function of $|H|$ for sample (a) NiS1 and (b) CFBS2 at room temperature. Magnetic field sweeps in both directions and field polarities are shown for field parallel (top) and perpendicular (bottom) to the long axis. We define H_d as the field at which most of the magnetization saturates and $\Delta R(H)/\Delta R_{max}$ is smaller than the noise level. For CFBS2, the saturation occurs at very small fields for the parallel field configuration.

min (R) is the minimum resistance value. The AMR ratio is defined as AMR $= \frac{R_\parallel - R_\perp}{R_\perp}$ where $R_\parallel$ and $R_\perp$ are the absolute maximum (max (R)) and minimum (min (R)) resistance values for a magnetic field H being parallel and perpendicular, respectively, to the current I and being larger than the field H_d at which most parts of the magnetization saturate.[34] Furthermore, we utilize the normalized resistance $\Delta R(H)/\Delta R_{max} = (R(H) - \min(R)) / (\max(R) - \min(R))$.

Before discussing the electrical properties and magnetoresistance of the nanotubes in detail, we determine H_d.[34] Magnetic field sweeps can be found in Fig. 3 for sample NiS1 (a) and CFBS1 (b) with H being parallel (top) and perpendicular (bottom) to the long axis (see supplementary material for further experimental data[29]). In the parallel configuration, only small fields were needed to saturate the nanotubes. CoFeB was in particular soft magnetic. In the perpendicular configuration, we extracted $\mu_0 H_d$ (black arrow) to be 0.35 ± 0.05 T for the Ni nanotube. This value was much smaller compared to the CoFeB nanotube for which we found 1.2 ± 0.2 T. We attribute this observation to different demagnetization fields. If we consider $M_s \approx 375$ kA/m for Ni,[22] we estimate the magnetometric demagnetization factor[34] to be $N_\perp(\text{Ni}) = |H_d(\text{Ni})/M_s(\text{Ni})| \approx 0.7$.[35] If we assume $N_\perp(\text{CoFeB}) = N_\perp(\text{Ni})$ and take the saturation magnetization of 1430 kA/m measured for our CoFeB when magnetron-sputtered on a planar substrate,[32] we calculate $\mu_0 H_d = \mu_0 N_\perp(\text{CoFeB}) \times M_s(\text{CoFeB}) \approx 1.3$ T. This value is consistent with the experimental value of $\mu_0 H_d = 1.2 \pm 0.2$ T observed for the CoFeB nanotube in Fig. 3(b). We do not expect the hexagonal shape of the smooth CoFeB nanotubes to

vary significantly the effective component of the demagnetization factor compared to the rougher and thereby more circular Ni nanotubes. The different values H_d thus reflect the different saturation magnetization values of Ni and CoFeB. Note that a large and thin film is expected to exhibit $N_\perp$ of 1.0 whereas an infinitely long (full) cylinder acquires $N_\perp = 0.5$. The extracted effective demagnetization factor of 0.7 for the nanotubes being hollow cylinders is in between these values and seems reasonable to us. The specific shape of the nanotubes reduces the overall demagnetization effect compared to a film, but still provides a larger effective demagnetization effect compared to a full cylinder. The nanobar-magnet behavior reported in Ref. 19 is consistent with the shape anisotropy provided by the relatively large $N_\perp \approx 0.7$ extracted here.

We now present the electrical properties and magnetoresistance of the nanotubes. Figure 4(a) shows the temperature dependent resistance $R(T)$ of a Ni nanotube (NiL1) at zero magnetic field. R decreases from 40.9 Ω at room temperature down to 15.8 Ω at 2 K. The behavior is expected for a polycrystalline metallic material. Using the geometrical parameters,[29] we calculate a specific resistivity $\rho = R \cdot A/L_{\text{contact}}$ of 18 $\mu\Omega$ cm and 7 $\mu\Omega$ cm for room and low temperature, respectively (A is the cross-section of Ni). Our values of ρ are in relatively good agreement with values measured on nanostripes fabricated from thermally evaporated Ni[36,37] indicating a good electrical quality of the ALD-grown metal. The temperature dependent $R(T)$ for two CoFeB samples is shown in Fig. 4(b). Here, we obtain specific resistivities of $\rho = 1 - 2 \times 10^3$ $\mu\Omega$ cm at room temperature. As a function of T we do not observe the typical metallic behavior. For sample CFBS1, the resistance decreases from room temperature down to 140 K and then increases. In case of CFBM1, the resistance increases monotonously with decreasing temperature. The measured resistances range from 7.63 to 7.79 kΩ and 7.35 to 7.79 kΩ for CFBS1 and CFBM1, respectively. The semi-logarithmic plot suggests $R(T)$ to exhibit a logarithmic dependence on $1/T$ for $T < T_{\text{min}} \approx 130$ K (190 K) for CFBS1 (CFBM1),[38] albeit a small deviation can be found for CFBM1 at $T < 10$ K.

Figure 4(c) shows the resistance change of Ni tubes as a function of the rotation angle θ at different temperatures. We rotated a field $H > H_d$ to saturate the tubes at all angles. $R(\theta)$ follows a $\cos^2(\theta)$ dependence remodelled by solid lines in Fig. 4(c). This is expected for ferromagnetic conductors displaying the AMR. Relative AMR values are shown in Fig. 4(d) as a function of T. Between 3 and 220 K, the AMR is found to increase linearly with T from about 0.35% to 1.2%. Then, up to 295 K, the AMR stays almost constant for sample NiL1. The low-temperature value is consistent with data obtained previously on different Ni nanotubes.[21] At room temperature, we now find a much larger value of up to 1.4% for NiS1 and NiM [Fig. 4(d)]. In Refs. 36 and 37, stripes from thermally evaporated Ni were studied and the authors provided values of 1.6% and 1.8%, respectively. We attribute the slightly smaller AMR effect of our nanotubes compared to the planar stripes mainly to the influence of the nanotube roughness. We assume the roughness-induced scattering of electrons to enhance the resistivity and thereby to reduce the overall AMR effect (compare considerations on boundary scattering in Ref. 39).

$R(\theta)$ of CoFeB nanotubes CFBS1 (triangles) and CFBM1 (squares) shown in Fig. 4(e) also follows a $\cos^2(\theta)$ dependence consistent with the AMR effect. The AMR effect is found to diminish with increasing T [Fig. 4(f)]. This is different from the Ni nanotubes. For CFBM1, we get AMR = 0.18% at 2 K and 0.08% at room temperature being more than an order of magnitude smaller than Ni. We attribute this to the amorphous structure of our unannealed CoFeB leading to a short electron mean free path and reducing the MR ratio.[40] The measured CoFeB resistivity of $1 - 2 \times 10^3$ $\mu\Omega$ cm is one order of magnitude larger compared to the best values given in literature for CoFeB alloy films with a comparable thickness.[41,42] For $R(T)$, we do not find a $T^{3/2}$ dependence in the accessible temperature range and rule out magnetic contributions to $R(T)$.[43] The characteristic minima in $R(T)$ [Fig. 4(b)] have been reported for many amorphous and granular alloys with intermediate resistivities[44,45] including CoFeB.[46,47] The following dependencies have been discussed for the low-temperature R when considering Coulomb interaction in disordered systems: $\exp(\sqrt{T_0/T})$,[48] a power law $1/T^\alpha$ or $\ln(T_0/T)$[38] (T_0 is a characteristic temperature and $0 < \alpha \ll 1$). The first (latter) occurs for systems with high (intermediate) resistivity.[38,46,49,50] Following Ref. 38, we attribute the logarithmic behavior of $R(T)$ in Fig. 4(b) for $T < T_{\text{min}}$ to electron-electron interaction in the disordered and amorphous material. The role of the columnar structure is not yet fully clear and under further investigation. Despite the complex $R(T)$ dependence, the AMR value of up to 0.18%

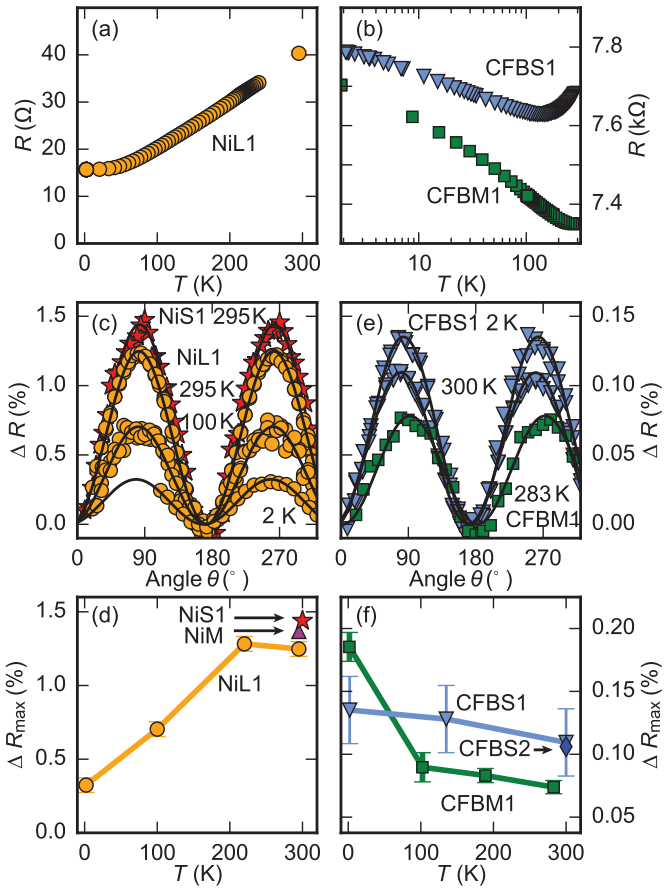

FIG. 4. Resistance R as a function of the temperature T for (a) the Ni nanotube NiL1 (circles) and (b) the two different CoFeB nanotubes CFBM1 (squares) and CFBS1 (triangles). For CoFeB, R is more than two orders of magnitude larger and shows a different temperature dependence (note the different axes) compared to the metallic Ni. (c) Resistance variation as a function of the angle θ displayed as $\Delta R(\theta)$ for NiL1 (circles) and NiS1 (stars) at 3 T and 2 T, respectively. The field values H were chosen such that $H > H_{sat}$ and magnetic saturation was achieved for all angles θ. (d) AMR ratios as a function of temperature for NiL1 (circles). For NiS1 (star) and NiM (triangle) room-temperature AMR ratios are given. (e) $R(\theta)$ of CFBS1 at 5 T at two temperatures (triangles) and CFBM1 at 2 T and 283 K. The data for CFS1 were taken in two-point configuration. (f) AMR ratios of samples CFBM1 (squares), CFBS1(triangles), and CFBS2 (diamond) at room temperature. The AMR effect of CFBM1 was extracted from magnetic field sweeps performed at different θ.[29] Solid lines in (c) and (e) indicate a $\cos^2(\theta)$ relationship. The maximum AMR ratio is one order of magnitude smaller for CoFeB compared to Ni.

that we observe for CoFeB nanotubes at small T is slightly larger than the value of 0.12% obtained by DFT simulations.[51]

The large room-temperature AMR ratios of up to 1.4% for Ni are encouraging for possible applications of nanotubes and, in general, magnetic devices on curved surfaces[7] prepared by ALD. Still there is room for improvement as the AMR ratio of bulk Ni is known to be 2%.[52] We expect an improved AMR ratio after reducing the surface roughness of the nickel. The smooth side facets of the CoFeB nanotubes make the integration of magnetic tunnel junctions[53] feasible, thereby enhancing the perspectives of nanotube-based sensing and local detection of domain walls.

In conclusion, we prepared nanotubes from Ni and CoFeB on non-magnetic nanotemplates using two different technologically relevant deposition techniques, i.e., atomic layer deposition and magnetron sputtering, respectively. Structural analysis of the CoFeB proved the shell to be amorphous. For polycrystalline Ni and amorphous CoFeB, the magnetic anisotropy was argued to be dominated by the shape. Both the relatively small resistivity and large AMR ratio of 1.4% obtained for Ni indicated a good electrical performance of the ALD-grown metal at room temperature. Magnetron-sputtered CoFeB nanotubes exhibited a much smoother surface but a smaller AMR effect

attributed to the amorphous structure and thereby enhanced electron scattering. The materials are highly eligible for magnetotransport studies on individual domain walls in nanotubes and nanotube-based sensing or logic applications. For room temperature spintronic applications, the relatively large AMR of Ni is promising. The larger saturation magnetization makes the CoFeB nanotubes favorable as magnetic tips in scanning probe microscopy.

The work has been supported by the DFG via GR1640/5-1 in SPP1538 "Spin caloric transport." Funding through the Swiss National Science Foundation NCCR QSIT and FP7 ITN Nanoembrace are greatly acknowledged. We acknowledge financial support from the European Union under a contract for an integrated Infrastructure Initiative 312483 - ESTEEM2 project that facilitates the use of advanced electron microscopes at ER-C Jülich. The authors would like to thank D. Meertens for the preparation of FIB lamellas. J.A. acknowledges the funding from the Spanish MICINN project MAT2010-15138 (COPEON), and Generalitat de Catalunya 2009 SGR 770. R.R.Z. acknowledges the former. The authors would also like to thank the TEM facilities in CCiT from Universitat de Barcelona.

[1] J. Escrig, P. Landeros, D. Altbir, E. Vogel, and P. Vargas, J. Magn. Magn. Mater. **308**, 233 (2007).
[2] P. Landeros, S. Allende, J. Escrig, E. Salcedo, D. Altbir, and E. E. Vogel, Appl. Phys. Lett. **90**, 102501 (2007).
[3] P. Landeros, O. J. Suarez, A. Cuchillo, and P. Vargas, Phys. Rev. B **79**, 024404 (2009).
[4] P. Landeros and A. S. Núñez, J. Appl. Phys. **108**, 033917 (2010).
[5] M. Yan, C. Andreas, A. Kákay, F. García-Sánchez, and R. Hertel, Appl. Phys. Lett. **99**, 122505 (2011).
[6] M. Yan, A. Kákay, C. Andreas, and R. Hertel, Phys. Rev. B **88**, 220412 (2013).
[7] S. S. P. Parkin, M. Hayashi, and L. Thomas, Science **320**, 190 (2008).
[8] N. S. Dellas, J. Liang, B. J. Cooley, N. Samarth, and S. E. Mohney, Appl. Phys. Lett. **97**, 072505 (2010).
[9] J. Liang, J. Wang, A. Paul, B. J. Cooley, D. W. Rench, N. S. Dellas, S. E. Mohney, R. Engel-Herbert, and N. Samarth, Appl. Phys. Lett. **100**, 182402 (2012).
[10] M. Hilse, Y. Takagaki, J. Herfort, M. Ramsteiner, C. Herrmann, S. Breuer, L. Geelhaar, and H. Riechert, Appl. Phys. Lett. **95**, 133126 (2009).
[11] A. Rudolph, M. Soda, M. Kiessling, T. Wojtowicz, D. Schuh, W. Wegscheider, J. Zweck, C. Back, and E. Reiger, Nano Lett. **9**, 3860 (2009), see http://pubs.acs.org/doi/pdf/10.1021/nl9020717.
[12] X. Yu, H. Wang, D. Pan, J. Zhao, J. Misuraca, S. von Molnár, and P. Xiong, Nano Lett. **13**, 1572 (2013), see http://pubs.acs.org/doi/pdf/10.1021/nl304740k.
[13] G. Tourillon, L. Pontonnier, J. P. Levy, and V. Langlais, Electrochem. Solid-State Lett. **3**, 20 (2000).
[14] J. Bao, C. Tie, Z. Xu, Q. Zhou, D. Shen, and Q. Ma, Adv. Mater. **13**, 1631 (2001).
[15] Y. C. Sui, R. Skomski, K. D. Sorge, and D. J. Sellmyer, Appl. Phys. Lett. **84**, 1525 (2004).
[16] K. Nielsch, F. J. Castaño, C. A. Ross, and R. Krishnan, J. Appl. Phys. **98**, 034318 (2005).
[17] M. Daub, M. Knez, U. Goesele, and K. Nielsch, J. Appl. Phys. **101**, 09J111 (2007).
[18] J. Bachmann, Jing, M. Knez, S. Barth, H. Shen, S. Mathur, U. Gösele, and K. Nielsch, J. Am. Chem. Soc. **129**, 9554 (2007).
[19] M. Hilse, J. Herfort, B. Jenichen, A. Trampert, M. Hanke, P. Schaaf, L. Geelhaar, and H. Riechert, Nano Lett. **13**, 6203 (2013).
[20] D. Zhang, Z. Liu, S. Han, C. Li, B. Lei, M. P. Stewart, J. M. Tour, and C. Zhou, Nano Lett. **4**, 2151 (2004).
[21] D. Rüffer, R. Huber, P. Berberich, S. Albert, E. Russo-Averchi, M. Heiss, J. Arbiol, A. Fontcuberta i Morral, and D. Grundler, Nanoscale **4**, 4989 (2012).
[22] D. P. Weber, D. Rüffer, A. Buchter, F. Xue, E. Russo-Averchi, R. Huber, P. Berberich, J. Arbiol, A. Fontcuberta i Morral, D. Grundler, and M. Poggio, Nano Lett. **12**, 6139 (2012), see http://pubs.acs.org/doi/pdf/10.1021/nl302950u.
[23] A. Buchter, J. Nagel, D. Rüffer, F. Xue, D. P. Weber, O. F. Kieler, T. Weimann, J. Kohlmann, A. B. Zorin, E. Russo-Averchi, R. Huber, P. Berberich, A. Fontcuberta i Morral, M. Kemmler, R. Kleiner, D. Koelle, D. Grundler, and M. Poggio, Phys. Rev. Lett. **111**, 067202 (2013).
[24] C. Butschkow, E. Reiger, A. Rudolph, S. Geißler, D. Neumaier, M. Soda, D. Schuh, G. Woltersdorf, W. Wegscheider, and D. Weiss, Phys. Rev. B **87**, 245303 (2013).
[25] H. Yu, R. Huber, T. Schwarze, F. Brandl, T. Rapp, P. Berberich, G. Duerr, and D. Grundler, Appl. Phys. Lett. **100**, 262412 (2012).
[26] J. Nagel, A. Buchter, F. Xue, O. F. Kieler, T. Weimann, J. Kohlmann, A. B. Zorin, D. Rüffer, E. Russo-Averchi, R. Huber, P. Berberich, A. Fontcuberta i Morral, D. Grundler, R. Kleiner, D. Koelle, M. Poggio, and M. Kemmler, Phys. Rev. B **88**, 064425 (2013).
[27] E. Uccelli, J. Arbiol, C. Magen, P. Krogstrup, E. Russo-Averchi, M. Heiss, G. Mugny, F. Morier-Genoud, J. Nygard, J. R. Morante, and A. Fontcuberta i Morral, Nano Lett. **11**, 3827 (2011).
[28] E. Russo-Averchi, M. Heiss, L. Michelet, P. Krogstrup, J. Nygard, C. Magen, J. R. Morante, E. Uccelli, J. Arbiol, and A. Fontcuberta i Morral, Nanoscale **4**, 1486 (2012).
[29] See supplementary material at http://dx.doi.org/10.1063/1.4891276 for an overview of relevant geometrical parameters of investigated nanotubes.
[30] M. de la Mata, C. Magen, J. Gazquez, M. I. B. Utama, M. Heiss, S. Lopatin, F. Furtmayr, C. J. Fernández-Rojas, B. Peng, J. R. Morante, R. Rurali, M. Eickhoff, A. Fontcuberta i Morral, Q. Xiong, and J. Arbiol, Nano Lett. **12**, 2579 (2012), see http://pubs.acs.org/doi/pdf/10.1021/nl300840q.

[31] A. T. Hindmarch, C. J. Kinane, M. MacKenzie, J. N. Chapman, M. Henini, D. Taylor, D. A. Arena, J. Dvorak, B. J. Hickey, and C. H. Marrows, Phys. Rev. Lett. **100**, 117201 (2008).
[32] T. Schwarze and D. Grundler, Appl. Phys. Lett. **102**, 222412 (2013).
[33] See http://www.qstarter.ch/projects/automated-contacting-of-random-microstructures.
[34] A. Aharoni, L. Pust, and M. Kief, J. Appl. Phys. **87**, 6564 (2000).
[35] Nanotubes are non-ellipsoidal magnetic elements for which an inhomogeneous internal field is expected when H is perpendicular to the long axis. This would make position-dependent demagnetization factors necessary when describing the micromagnetic behavior in detail. This is why we define the so-called magnetometric demagnetization factor.
[36] D. Rüffer, F. D. Czeschka, R. Gross, and S. T. B. Goennenwein, Appl. Phys. Lett. **99**, 142112 (2011).
[37] Y. Q. Jia, S. Y. Chou, and J.-G. Zhu, J. Appl. Phys. **81**, 5461 (1997).
[38] K. B. Efetov and A. Tschersich, Phys. Rev. B **67**, 174205 (2003).
[39] T. G. S. M. Rijks, R. Coehoorn, M. J. M. de Jong, and W. J. M. de Jonge, Phys. Rev. B **51**, 283 (1995).
[40] S. Tsunashima, M. Jimbo, Y. Imada, and K. Komiyama, J. Magn. Magn. Mater. **165**, 111 (1997).
[41] Y.-T. Chen and S. M. Xie, J. Nanomater. **2012** (2012).
[42] S. U. Jen, Y. D. Yao, Y. T. Chen, J. M. Wu, C. C. Lee, T. L. Tsai, and Y. C. Chang, J. Appl. Phys. **99**, 053701 (2006).
[43] S. N. Kaul, W. Kettler, and M. Rosenberg, Phys. Rev. B **33**, 4987 (1986).
[44] O. Touraghe, M. Khatami, A. Menny, H. Lassri, and K. Nouneh, Physica B **403**, 2093 (2008).
[45] S. N. Kaul, W. Kettler, and M. Rosenberg, Phys. Rev. B **35**, 7153 (1987).
[46] H. Fujimori, S. Mitani, T. Ikeda, and S. Ohnuma, IEEE Trans. Magn. **30**, 4779 (1994).
[47] G. V. Swamy, H. Pandey, A. K. Srivastava, M. K. Dalai, K. K. Maurya, Rashmi, and R. K. Rakshit, AIP Adv. **3**, 072129 (2013).
[48] A. L. Efros and B. I. Shklovskii, J. Phys. C: Solid State Phys. **8**, L49 (1975).
[49] T. Chui, G. Deutscher, P. Lindenfeld, and W. L. McLean, Phys. Rev. B **23**, 6172 (1981).
[50] R. W. Simon, B. J. Dalrymple, D. Van Vechten, W. W. Fuller, and S. A. Wolf, Phys. Rev. B **36**, 1962 (1987).
[51] K. M. Seemann, F. Freimuth, H. Zhang, S. Blügel, Y. Mokrousov, D. E. Bürgler, and C. M. Schneider, Phys. Rev. Lett. **107**, 086603 (2011).
[52] T. McGuire and R. Potter, IEEE Trans. Magn. **11**, 1018 (1975).
[53] S. Ikeda, K. Miura, H. Yamamoto, K. Mizunuma, H. D. Gan, M. Endo, S. Kanai, J. Hayakawa, F. Matsukura, and H. Ohno, Nat. Mater. **9**, 721 (2010).